










Internal Gas Composition and Pressure in As-drawn Hollow Core Optical Fibers

Shuichiro Rikimi , Yong Chen, *Member, IEEE*, Thomas W. Kelly , Ian A. Davidson, Gregory T. Jasion , *Member, IEEE*, Matthew Partridge, Kerriane Harrington, Thomas D. Bradley , *Member, IEEE*, Austin A. Taranta , Francesco Poletti , *Member, IEEE*, Marco N. Petrovich , *Senior Member, IEEE*, David J. Richardson , *Fellow, IEEE*, and Natalie V. Wheeler , *Senior Member, IEEE*

Abstract—We present a study into the gas pressure and composition within a hollow core optical fiber immediately after fabrication. Results from three different experimental techniques indicate that the initial absolute pressure inside of the hollow core is significantly lower than atmospheric pressure. By measuring the equilibrium height to which water ingresses into the hollow core, we estimate the absolute internal gas pressure to be $20 \text{ kPa} < P_i < 29 \text{ kPa}$ for the fibers reported here that were fabricated using standard techniques. The initial gas composition within the hollow core was studied using Raman and absorption spectroscopy and the evolution of the gas composition provides indirect information about the condition of the silica surfaces inside the fiber. The measurements indicate that these internal surfaces become saturated with atmospheric water vapor as this is drawn into the open-ended fiber, initially due to a pressure gradient post-fabrication. Our findings are an essential foundation for the study of long-term optical and mechanical performance of hollow core fibers and important for accurate characterization of these specialty fibers. The first is becoming increasingly important as commercial applications of these fibers expand.

Index Terms—Glass, optical fiber applications, optical fiber measurements, optical fibers.

I. INTRODUCTION

OPTICAL fibers are a key enabling technology across a multitude of industries and in everyday life. For example,

Manuscript received September 23, 2021; revised December 26, 2021 and February 9, 2022; accepted March 29, 2022. Date of publication April 5, 2022; date of current version July 16, 2022. The work of Natalie V. Wheeler was supported by Royal Society. The work of Francesco Poletti was supported by ERC project LightPipe under Grant 682724. This work was supported in part by Lumenity Ltd., EPSRC Programme under Grant AirGuide Photonics EP/P030181/1, and in part by the EPSRC National Hub in High Value Manufacturing under Grant EP/N00762X/1. (*Corresponding author: Shuichiro Rikimi.*)

Shuichiro Rikimi, Thomas W. Kelly, Ian A. Davidson, Gregory T. Jasion, Matthew Partridge, Kerriane Harrington, Thomas D. Bradley, Austin A. Taranta, Francesco Poletti, David J. Richardson, and Natalie V. Wheeler are with the Optoelectronics Research Centre, University of Southampton, SO17 1BJ Southampton, U.K. (e-mail: sr1y15@soton.ac.uk; twk1g15@soton.ac.uk; i.a.k.davidson@soton.ac.uk; g.jasion@soton.ac.uk; m.c.partridge@soton.ac.uk; k.harrington@soton.ac.uk; t.bradley@soton.ac.uk; a.a.taranta@soton.ac.uk; frap@orc.soton.ac.uk; djr@orc.soton.ac.uk; nvw1v10@orc.soton.ac.uk).

Yong Chen and Marco N. Petrovich are with the Optoelectronics Research Centre, University of Southampton, SO17 1BJ Southampton, U.K., and also with Lumenity Ltd., Unit 7, The Quadrangle, Premier Way, SO51 9DL Romsey, U.K. (e-mail: yc1m12@soton.ac.uk; mnp@orc.soton.ac.uk).

This article has supplementary material provided by the authors and color versions of one or more figures available at <https://doi.org/10.1109/TEM.2022.3158398>.

Digital Object Identifier 10.1109/JLT.2022.3164810

they underpin modern communications, provide essential beam delivery as endoscopes for medical diagnosis and treatment and enable distributed sensing across various platforms [1], [2]. Conventional all-solid fibers, based on total internal reflection, are the most familiar fibers in current applications. Even with their tremendous success, these conventional fibers do have limitations, mainly due to the interaction of the guided light with the solid glass material that forms the fiber core; these limits are now holding back some next generation systems. Hollow core optical fibers (HCFs) are alternative, specialty optical fibers that are now emerging as a viable candidate to overcome some of these limitations. In a HCF, light can propagate in an air-core confined by an appropriately designed, microstructured cladding [3], [4]. As such, HCFs have several advantages compared to conventional fibers such as ultra-low loss [5], low latency [6], low non-linearity [7], exceptional polarization purity [8], high threshold to laser-induced damage [9] and low thermal sensitivity [10], and their potential in real world network deployments is currently being demonstrated [11].

Long-term reliability and performance consistency are a critical consideration for any practical technology. Aging forms one aspect of this; the aging mechanisms of solid-core fibers have been extensively investigated to enable stable performance even in submarine environments for more than 25 years [12], [13]. Although HCFs are usually fabricated using a similar grade of silica glass as conventional all-solid fibers, the presence of the internal microstructure, with its large internal surface that extends longitudinally along the full fiber length, is likely to substantially influence the aging process, potentially influencing fatigue of mechanical strength due to water vapor, as observed in silica solid core fibers [14], and the consistency of HCF's optical properties, such as loss degradation. Various factors could be important here, such as the presence of several gas species within the microstructure, the change in the composition of these species over time, and their interactions at the large glass-gas interfaces within the microstructure. Previous studies have reported the observation of atmospheric gas species (e.g., water vapor, carbon dioxide [15]) as well as other gas species such as hydrogen chloride within the hollow core, which originate from the raw silica glass used to fabricate the HCF [16].

However, prior to beginning an investigation into aging effects in HCFs, there is an important question which at this point has

not been fully investigated: what are the internal conditions of a HCF immediately post-fabrication? Important factors could include the initial gas composition, pressure and its interaction with the internal silica surfaces. Defining the initial condition will enable identification of changes in the HCF condition related to long-term optical performance and open up possibilities to mitigate any observed degradation mechanisms, potentially providing a basis to define storage and handling procedures of HCFs post-fabrication. Furthermore, the gas composition and its evolution could impact the performance of HCFs in spectral regions where gases inside the fiber have absorption features; for example, water vapor absorption can increase loss in the wavelength range between ~ 1300 and 1500 nm; a spectral range where HCFs could have impact in future transmission systems.

Recently we reported a preliminary study into the internal pressure within a HCF which indicated that the gas pressure within a HCF immediately after fabrication is significantly below atmospheric pressure [17]. Here we build on this work. The initial gas pressure inside a HCF post-fabrication is studied using three methods: absorption spectroscopy, Raman spectroscopy and detection of the moving meniscus as liquid water ingresses into the hollow core. The gas absorption and Raman spectroscopy measurements are used to examine the evolution of gas concentration inside a hollow core -photonic bandgap fiber (HC-PBGF) and a tubular hollow core antiresonant fiber (HC-ARF), both of which show an initial fast ingress of gas upon exposure to atmosphere, which is much faster than expected from diffusion alone. In fact, we show good agreement with a pressure-driven gas flow model; the results indicate that the pressure inside a HCF post-fabrication must be significantly below atmospheric pressure. Subsequent measurements of pressure-driven liquid water flow inside the HCF enabled us to estimate the initial absolute pressure to be between 20 kPa and 29 kPa. We also observed evidence that water vapor has high affinity to the inner glass surfaces of an ‘as-drawn’ HCF, whereas oxygen and nitrogen seem not to interact with the surfaces. The large pressure difference accelerates the ingress of the atmosphere, including water vapor, which potentially affects the optical properties and the mechanical lifetime of the HCF. This implies that sealing the HCF after fabrication or exposing the fiber ends to a carefully controlled inert atmosphere could be beneficial.

This paper is separated into five sections. In Section II, the fibers used in this work are described in detail and we introduce the term ‘as-drawn’ fibers. Experimental techniques and results are described and compared with theoretical models in Section III. In Section IV, the key results and possible reasons for the pressure difference are discussed, and the paper is concluded in Section V.

II. FIBER FABRICATION AND CHARACTERISATION

HCFs are typically fabricated using the stack and draw technique [3]. Here, up to several hundred capillaries ($\sim 2\text{--}3$ mm in diameter) are assembled into the desired arrangement and inserted into a jacketing tube. This stack forms the initial HCF preform which is then usually drawn to a fiber in two stages. In the first drawing stage, this initial preform is drawn under carefully controlled conditions into canes which are a few mm

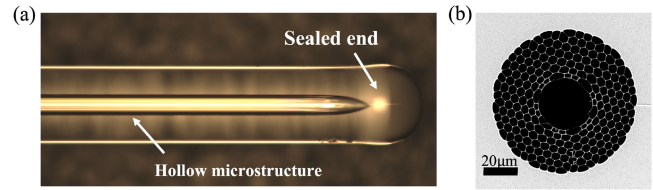


Fig. 1. (a) An optical image of a sealed end of a HCF. The bright part in the middle is a hollow microstructure which is collapsed at one end. (b) A SEM image of the HC-PBGF used for the gas absorption measurement.

in diameter. Then, the cane material is inserted in a further jacket tube to form the second preform and drawn into a fiber. During the fiber drawing process, inert gas is used to pressurize the cane in order to control the final fiber geometry. Therefore, depending on the fabrication parameters, it may be expected that the gas content within an as-drawn HCF will include both air constituents and the inert pressurization gas.

In this work, all the HCFs used are ‘as-drawn’ fibers; we use this term to describe fibers which are sealed at both ends using an arc-fusion splicer immediately after fiber drawing (< 5 minutes after the fabrication of that specific fiber has finished) in order to minimize inflow or outflow of gasses between the holes in the microstructure and the surrounding atmosphere and to therefore preserve the gas concentration and pressure within the HCF immediately after fabrication. Fig. 1(a) shows an image of the end of a HCF collapsed using an arc-splicer. The HCFs used in experiments were all fabricated using Heraeus F300 material which contains a relatively high concentration of chlorine (800–2000 ppm) [18].

After the fiber ends were sealed, the HCFs were carefully stored in a laboratory and therefore the as-drawn condition was preserved until measurements were taken. The sealed ends were then cleaved immediately prior to the experiments described in this paper. The initial internal conditions of the as-drawn fiber were evaluated here by two different methods: (i) optically monitoring changes in gas concentration and (ii) measuring the height of liquid water rising in the core. Both methods are dependent on the internal condition of the HCF because the dynamics of their flow depends on internal pressure.

III. EXPERIMENTAL RESULTS AND ANALYSIS

The following section is divided into three parts: gas absorption spectroscopy, Raman spectroscopy, and ingress of liquid water measurements. In each sub-section, the experimental procedures are explained and experimental results are shown. The results are discussed along with calculations in order to assess the internal conditions in an as-drawn HCF.

A. Gas Absorption Spectroscopy Measurement

In our first experiment, the evolution of water vapor concentration inside a 19-cell HC-PBGF was measured using gas absorption spectroscopy, in order to probe the internal pressure in an as-drawn fiber and to study water vapor behavior in HCFs. A scanning electron microscope (SEM) image of the HC-PBGF used here is shown in Fig. 1(b); the design of this structure is the same as that reported in [19] and the core diameter is $31.6 \mu\text{m}$.

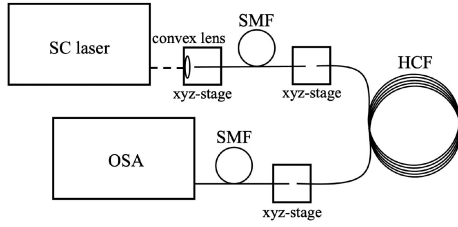


Fig. 2. Experimental set-up of the absorption spectroscopy measurement. The components shown are a supercontinuum laser (SC laser), a xyz-stage, a single-mode fibre (SMF), a hollow core fibre (HCF), and an optical spectrum analyser (OSA).

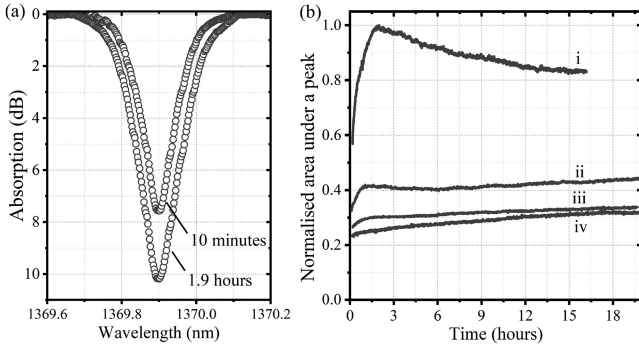


Fig. 3. (a) Absorption of water vapor at 1369.9 nm at 10 minutes and 1.9 hours after opening the fiber ends. (b) Evolution of the measured water vapor absorption in the HC-PBGF: (i) the first run, (ii) the second run, (iii) the third run and (iv) the fourth run.

Fig. 2 is a schematic of the experimental set-up. Light from a supercontinuum laser (SC Fianium SC400) was launched into a single mode fibre (SMF) via an objective lens and the output was coupled into 55 m of the HC-PBGF. The transmission through the HCF was collected by an SMF and recorded using an optical spectrum analyzer (OSA Yokogawa AQ-6315A) with 0.05 nm resolution to resolve water vapor absorption lines. At the interfaces between the HCF and the SMFs, the fibers were butt-coupled with a ~ 3 mm gap (using xyz alignment stages) to allow air access to the hollow core from both ends. The as-drawn HC-PBGF was aligned in the optical setup immediately after opening the fiber ends (by cleaving off the sealed tips); the alignment of the HCF took approximately 10 minutes and then transmission spectra through the fiber were continuously recorded using the OSA for more than 16 hours. After the measurement, the fiber ends were sealed again and the fiber stored for two weeks until the next measurement. The experiment was subsequently repeated three more times using the same setup and procedure.

To analyze the water vapor dynamics, the absorption line at 1369.9 nm was selected because of its suitable absorption strength and isolation from adjacent absorption lines. The absorption was evaluated by the integral of the peak as shown in Fig. 3(a). Since water vapor exists in the light path between the SC and OSA, this background absorption level was recorded without the HC-PBGF in the set-up at the beginning and end of each measurement and subtracted from the HC-PBGF measurement.

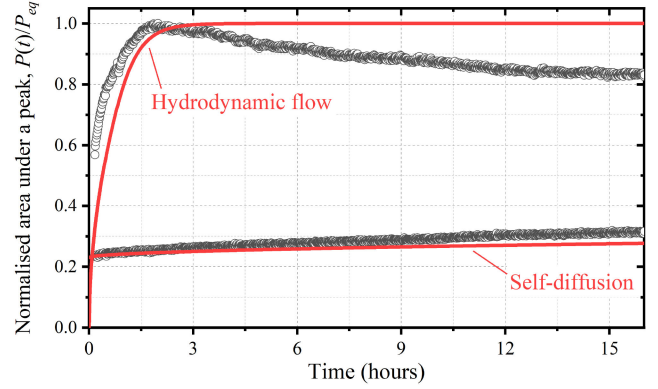


Fig. 4. Comparison of the first run and the fourth run shown in Fig. 3 with numerical solution of pressure-driven gas flow of (1) and self-diffusion of (2) with 0.23 offset to be compatible with the fourth run experimental result.

Fig. 3(b) shows the evolution of the water vapor absorption for the four experiments, where the observed absorption in each case has been normalized by the maximum value in the 1st run. Two clear trends were observed from the first run; firstly, the absorption increased very quickly over time up to ~ 1.9 hours after opening the ends, and then secondly, it slowly decayed. Although similar features were shown in the second run, the rate of increase and the decay effect were both smaller than observed in the 1st run. In the third run, these features were weaker still and in the final test, the observed absorption just increased slowly with time. One feature observed for all tests was that the absorption at the beginning of the measurement was always below that at the end of the previous measurement.

The initial significant change in the 1st run implies that the water vapor was driven into the HCF not only by diffusion but also by another force. The diffusion equation, as modified for pressure-driven gas flow in the hydrodynamic regime using Hagen-Poiseuille flow [20], is given by

$$\frac{\partial P}{\partial t} = \frac{r^2}{8\mu} \frac{\partial}{\partial x} \left(P \frac{\partial P}{\partial x} \right) \quad (1)$$

where r , P , μ , t and x are the core radius, the pressure inside the fiber, the dynamic viscosity, the time and the position along the fiber, respectively. By numerically solving (1), the distribution of the gas pressure along the fiber at an arbitrary time is obtained and can be compared with our experimental results by integrating along the length of the fiber, L (see supplementary material for a more detailed discussion). In Fig. 4, the evolution of the water vapor concentration in the 1st run is compared with (1) using the fiber parameters: $2r = 31.6 \mu\text{m}$ and $L = 55$ m. In this experiment, the water vapor was transported into the HCF as a component of the atmospheric gas composition and hence, for comparison with the experimental result, the dynamic viscosity of air was used in (1) ($\mu_{\text{air}} = 1.8192 \times 10^{-5} \text{ kg/(m}\cdot\text{s)}$ [21]) and the filling pressure was set $P_{\text{fill}} = 1$ standard atmosphere (atm.) because atmospheric gas entered the HCF from the surrounding atmosphere via the two open fiber ends. In [20], (1) is applied considering an absolute initial pressure inside the hollow core $P_0 = 0$ Pa, while in our experiment, this initial pressure was unknown. However, we found that using as $P_0 = 0$ Pa as a first

estimate of the internal pressure gives a reasonable agreement between the numerical model and the experimental data for the peak time of the 1st run. This indicates that the internal pressure in the as-drawn condition was significantly below atmospheric pressure. As discussed in Section IV, the discrepancy between the pressure-driven gas flow model and the 1st run (particularly after the peak concentration time) is highly likely attributed to adsorption processes of water vapor onto the silica surfaces defining the hollow core. The adsorption effect is not considered in the model of (1).

According to this result, the different behaviors observed in the second to fourth runs could be attributed to the progressively reducing pressure difference between the gas inside the HCF and the external environment upon each subsequent opening of the fiber ends. Given enough time, we would expect the gas pressure inside the HCF to equalize with the atmospheric pressure in the external environment, at which point any changes in the concentration of species would be governed by diffusion. When the gas moves into the fiber by only diffusion (in the absence of any pressure gradient), the time dependent average gas density, $n(t)$, is expressed as [20]:

$$\begin{aligned} \frac{n(t)}{n_{eq}} &= \frac{P(t)}{P_{eq}} \\ &= 1 - \frac{8}{\pi^2} \sum_{j=0}^{\infty} \frac{1}{(2j+1)^2} \exp \left\{ \left[\frac{(2j+1)\pi}{L} \right]^2 Dt \right\} \end{aligned} \quad (2)$$

where D and j are the self-diffusion coefficient and integer in the summation, respectively, and the subscript eq represents the equilibrium state. The ideal gas law, $n = P/k_B T$, is applied in (2) and the diffusion coefficient of water vapor in air at 20 °C is calculated to be $D = 2.42 \times 10^{-5} \text{ m}^2/\text{s}$ [22]. The comparison between (2) using this diffusion coefficient, and the experimental result from the fourth run in Fig. 4 indicates that the gas flow dynamics had gradually transitioned to the self-diffusion regime from ingress through the open fiber ends in previous runs, and this resulted in the decrease in the water vapor uptake rate.

B. Raman Spectroscopy Measurement

The water vapor absorption measurements strongly indicate that the gas inside as-drawn HCFs is at sub-atmospheric pressure. In our second experiment, the initial gas concentration and pressure inside a tubular HC-ARF [23] was investigated using gas-phase Raman spectroscopy. The broad transmission bandwidth, combined with the low loss of the fiber used here, enables simultaneous detection of several gas species including water vapor as well as oxygen and nitrogen. Such non-polar molecules will allow observation of the effect of the differential pressure with negligible interactions with the silica surface.

The experimental set-up is explained in Fig. 5. The pump light source is a 532 nm Coherent Sapphire laser; the output of this laser is reflected by a dichroic mirror (DM) and launched into the HCF through an aspheric lens (AL). The backscattered Raman Stokes signals propagate back within the hollow core and through the lens system before being collected by the spectrometer via a multimode fiber (MMF). Any residual pump light

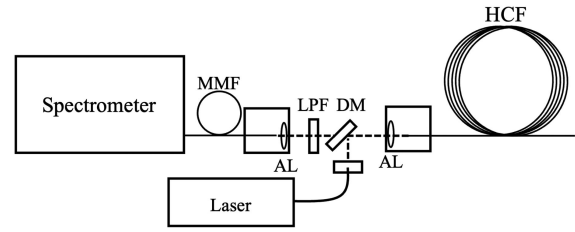


Fig. 5. Experimental set-up of the Raman spectroscopy measurement. HCF, DM, AL, LPF and MMF represent the hollow core fibre, the dichroic mirror, the aspheric lens, long-pass filter, the multimode fiber and the spectrometer, respectively.

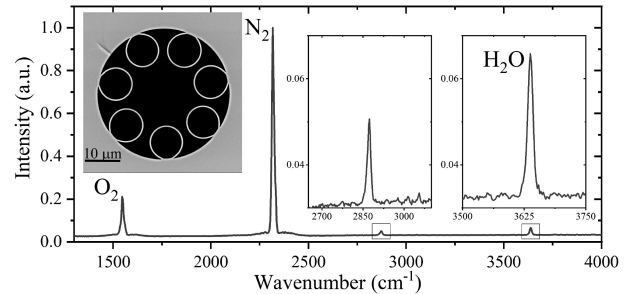


Fig. 6. The Raman Stokes signatures of oxygen, nitrogen, water vapor and another, not definitively identified, gas species at 2873 cm^{-1} through the tubular AR-HCF 21 minutes after cleaving of the fiber end. The inset is a SEM image of the HCF.

present before the MMF is removed by a long-pass filter (LPF). The spectrometer can detect Raman Stokes signals between 1300 cm^{-1} and 4000 cm^{-1} with a resolution of $\sim 4 \text{ cm}^{-1}$ and acquisition time of ~ 5 seconds. As with the experiments described above, experimental data was recorded as soon as possible after cleaving the HCF ends, 21 minutes in the measurement reported here. The Raman spectra recorded from the HC-ARF 21 minutes after cleaving off the sealed fiber ends is shown in Fig. 6 with the inset of a SEM image of the HC-ARF used; the core diameter and the length of the HC-ARF were 18.5 μm and 34 m, respectively. Four peaks were observed from the spectrum, corresponding to oxygen (1546 cm^{-1}), nitrogen (2316 cm^{-1}), water vapor (3637 cm^{-1}) and a further species which does not originate from the atmosphere (2873 cm^{-1}). The concentration evolution of the water vapor, oxygen and nitrogen up to 60 hours after opening the HCF ends is shown in Fig. 7(a)–(c); note that the small oscillations on the experimental data was due to the temperature fluctuation in the laboratory. The Raman signals are normalized to the stabilized maximum value which occurs at 2.35 hours for the water vapor and 3.5 hours for the oxygen and nitrogen.

The water vapor showed the same features as those observed in the absorption spectroscopy experiment with the HC-PBGF, albeit with a different time scale due to the difference in fiber geometry and length. Here, again the signal of the water vapor initially increased (up to about 2.35 hours) and then gradually decreased. The rate of reduction for the water vapor was higher in the HC-ARF than the HC-PBGF. This could potentially be attributed to the large inner surface area surrounding the hollow core; the inner core surface area of the HC-ARF used here is ~ 3.5 times larger (due to the non-circular core shape) than that of the HC-PBGF studied in Section III A.

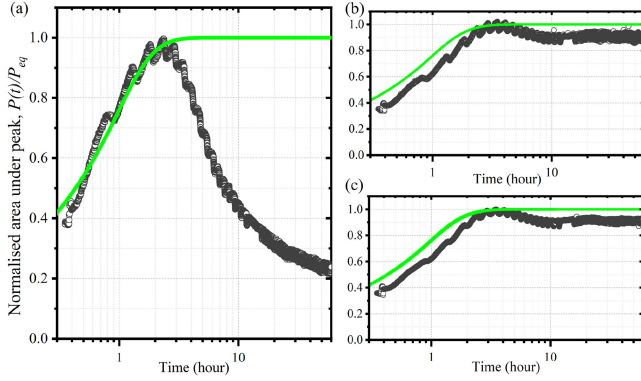


Fig. 7. Evolution of the Raman Stokes signal of (a) water vapor, (b) oxygen and (c) nitrogen. The green solid line is the numerical solution of (1) using $P_0 = 0$ and the experimental parameters described in the main text.

On the other hand, the filling time of the oxygen and nitrogen was about 3.5 hours and the signal decay observed for the water vapor was not seen and, after the initial increase, their concentration within the hollow core was stable over the 60 hours of measurement. The differences observed between the water vapor and the nitrogen and oxygen gases were most probably due to degree of interaction of the different gases with the inner silica surface of the HCF (see Section IV for further discussion). The small reduction in the Raman signals observed after 3.5 hours for the oxygen and nitrogen can be due to different average gas pressures inside the hollow core and the cladding tubes as the pressure inside the microstructured regions equalizes to atmospheric at different rates due to the different hole sizes. This was reported in a recent HCF-based Raman gas sensing study [24] in which similar transient behavior in the Raman signal was observed using a tubular HC-ARF during gas filling.

The model described by (1) was used again with the following parameters: $2r = 18.5 \mu\text{m}$, $L = 34 \text{ m}$, $\mu_{\text{air}} = 1.8192 \times 10^{-5} \text{ kg/(m}\cdot\text{s)}$, $P_0 = 0 \text{ Pa}$ and $P_{\text{fill}} = 1 \text{ atm.}$, and the predictions from the model are plotted along with the experimental results in Fig. 7(a)–(c). Again, we applied (1) assuming an initial internal gas pressure of 0 Pa, and in this case, the theory agrees well with the experiments; in particular, the peak time of the oxygen and nitrogen reasonably matches with that of the calculation. This provides further evidence that the internal pressure post-fabrication is much lower than the atmosphere, close to 0 Pa. The small discrepancy between the model and the oxygen/nitrogen behaviors could be due to: (i) the pressure-driven gas flow model was built for a circularly shaped tube [20] and (ii) the actual initial internal pressure (P_0) was close to but not exactly 0 Pa.

In addition to the atmospheric gasses, the peak at 2873 cm^{-1} was observed just after opening the fiber ends and this indicates that the gas species originated from the fiber itself. Calibration of the detected O_2 and N_2 peak position with reference values (1555 cm^{-1} and 2331 cm^{-1} for O_2 and N_2 , respectively [25]) suggests that the undefined peak is attributed to hydrogen chloride gas (HCl) which has a Q-branch peak at 2886 cm^{-1} [26], [27]; see Section IV for further discussion regarding the origin of this peak. The time dependence of the Raman Stokes signal is under further investigation.

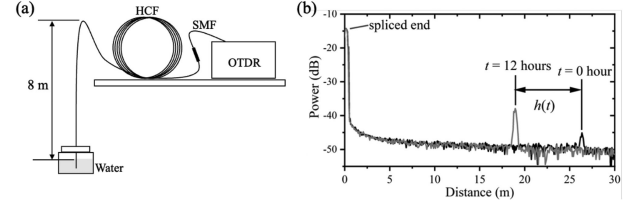


Fig. 8. (a) Experimental set-up of the liquid water flow measurement using OTDR. (b) The OTDR traces of the HC-PBGF A at $t = 0$ hour and $t = 12$ hours after loading into the liquid water.

C. Pressure-driven Liquid Water Flow Measurement

The observed changes in gas concentration provide strong evidence of low internal gas pressure inside as-drawn HCFs. In this section we complement these results with a fluid mechanical measurement which provides information on the absolute pressure within the hollow core by introducing liquid water and tracking its ingress. The equilibration of forces acting on this liquid inside the fiber provides a measure of the difference between internal and external pressure.

Here, the consideration of capillary action in a vertical tube [28] is extended to include the situation where the internal pressure differs from atmospheric pressure by ΔP (see supplementary material for a more detailed discussion). Under static conditions, the force balance on the meniscus is given by

$$\frac{2\gamma\cos\theta}{r} + \Delta P = \rho gh_{\text{eq}} \quad (3)$$

where ρ , γ , θ , g , h_{eq} and r are the density of the liquid, the surface tension of the liquid, the contact angle between the liquid and the solid surface, the acceleration due to gravity, the equilibrium height of the liquid and the tube radius, respectively.

To measure the movement of liquid water inside the hollow core we use optical time domain reflectometry (OTDR, LOR200). While OTDR is conventionally applied to optical fibers for loss and defect measurements, as water ingresses into the hollow core, the air-water interface inside the hollow core causes a measurable reflection of input light which can be detected by the OTDR. The set-up for this experiment is shown in Fig. 8(a). Two HC-PBGFs were prepared for this experiment: HC-PBGF A and HC-PBGF B which had the same microstructure as shown in Fig. 1(b). The former was an as-drawn fiber and the later was an atmospheric-pressure fiber. For the as-drawn pressure measurement, 26.5 m of HC-PBGF A was used, with $\sim 18 \text{ m}$ wound on a bobbin and 8 m suspended vertically in a straight length. In order to maintain the as-drawn pressure inside the HCF during the measurement, the HCF end connected to the OTDR was spliced to an all-solid large mode area fiber and a SMF pigtail in advance; the HCF end was exposed to atmosphere for ~ 3 mins during this process. A container filled with deionized water (liquid) was placed near the lower end of the HCF and this distal end of the HCF was loaded into the water immediately after cleaving off the sealed tip. OTDR traces, examples of which are shown in Fig. 8(b), were then recorded every 2 minutes for a total time period of 40 hours. The height of the water rises inside the HCF as a function of time was then

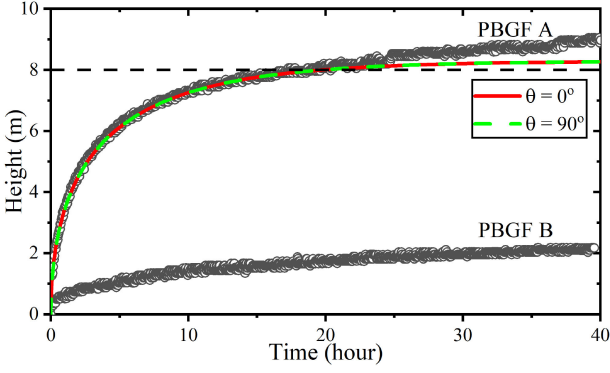


Fig. 9. Time variation of the rising water level inside the as-drawn PBGF A and the atmospheric-pressure PBGF B. The green dashed and red solid lines are the numerical calculation of (4) with $(\theta, \Delta P) = (90^\circ, 81 \text{ kPa})$ and $(0^\circ, 72 \text{ kPa})$, respectively, and the parameters described in the main text. The dashed black line highlights $h = 8 \text{ m}$ at which PBGF A started to bend.

deduced from the OTDR traces. The capillary rise height is given by $h(t) = (t) - d_0$ where d_0 and (t) are the observed distances to the reflection point at the end of the fiber, as measured at time $t = 0$ and during the experiment due to the air-water interface, respectively. d_0 was measured before loading the HCF into the water. The wavelength and pulse width of the probe laser within the OTDR were 1550 nm and 2 ns, respectively. The surface tension, density and dynamic viscosity of liquid water used for the calculations below are $\gamma = 72.75 \times 10^{-3} \text{ N/m}$, $\rho = 998.2 \text{ kg/m}^3$ and $\mu = 1.002 \times 10^{-3} \text{ kg/(m}\cdot\text{s)}$, respectively [29]–[31].

The deduced rise of water within the as-drawn HC-PBGF A is shown in Fig. 9 and compared with a result obtained using a 20 m length of HC-PBGF B, that was left in the atmosphere with open ends for two weeks before testing. According to (1), this 20m length would have been completely filled with air in ~ 40 minutes when $P = 1 \text{ atm.}$ and $P_0 = 0 \text{ Pa}$, and therefore two weeks exposure to air is more than enough to ensure atmospheric pressure inside the hollow core. A dramatic change was observed in the as-drawn fiber; the water rose up to 8.0 m over the 20 hours. On the other hand, in the atmospheric-pressure fiber the water level was only found to increase relatively slowly and the height at 20 hours was 1.7 m, which was significantly lower than that of the as-drawn fiber.

The dramatic change in the height of the liquid in the as-drawn fiber can be attributed to the pressure difference inside the HCF compared to the atmosphere, and the experiment showed that h_{eq} was above 8.0 m (the position at which the as-drawn fiber was bent within the experimental set-up). To estimate h_{eq} from the experimental data, capillary flow in a cylindrical tube, expressed by the Newtonian dynamics equation [28], can be modified to introduce pressure-driven liquid flow:

$$\rho\pi r^2 \frac{\partial}{\partial t} \left(h(t) \frac{\partial h(t)}{\partial t} \right) = \pi r^2 \frac{2\gamma \cos\theta}{r} - \pi r^2 h(t) \rho g - 8\pi\mu h(t) \frac{\partial h(t)}{\partial t} + \pi r^2 \Delta P \quad (4)$$

In (4), the left-hand side represents the inertia force and the terms on the right-hand side of the equation represent the forces

due to surface tension, gravity, viscous shear stress and pressure difference, respectively. The pressure difference is assumed to be constant over time and any evaporation of the liquid water inside the fiber is not considered. Here, a numerical calculation of (4) was compared with the experimental data between $h = 0 \text{ m}$ and $h = 8 \text{ m}$ by changing ΔP for two fixed contact angles of $\theta = 0^\circ$ and 90° ; both extremes of the contact angle were considered here due to the uncertainty of the inner silica surface conditions [32], [33]. ΔP was determined using a least squares method for different r . In Fig. 9, the pressure-driven capillary flow in the as-drawn fiber showed the best fit with the numerical calculation using $(\theta, \Delta P) = (90^\circ, 81 \text{ kPa})$ or $(0^\circ, 72 \text{ kPa})$ for $r = 15.1 \mu\text{m}$; both sets gave similar dynamics. The slightly smaller core radius found for the calculation could be due to the non-perfect circularly shaped core as seen from the SEM image in Fig. 1(b) and the effect of dynamic contact angle [28]. h_{eq} estimated from the numerical results was 8.29 m for both sets and the upper limit of h_{eq} predicted using (3) with $\Delta P = 1 \text{ atm.}$, $\theta = 0^\circ$ and $r = 15.8 \mu\text{m}$, gives the maximum $h_{eq} = 11.3 \text{ m}$, indicating that the estimated h_{eq} appears reasonable.

The results of $72 \text{ kPa} < \Delta P < 81 \text{ kPa}$ with the uncertainty of $0^\circ < \theta < 90^\circ$ imply that the absolute initial pressure inside the hollow core is $20 \text{ kPa} < P_i < 29 \text{ kPa}$, which is about one quarter of atmospheric pressure. Since the fiber was exposed to the atmosphere during the splicing process, ΔP immediately post-fabrication is likely to be higher (and P_i lower) than that implied by this experiment. This quantitative estimation of the internal gas pressure is in reasonable agreement with that indicated by the gas spectroscopy measurements and, to our knowledge, is the first time that the internal pressure inside a HCF post-fabrication has been estimated.

IV. DISCUSSION

A. Prediction of the As-Drawn Pressure

As mentioned in Section II, the different HCFs in this work were all fabricated via the conventional two-stage stack and draw technique [3]. A key difference between the fabrication of all-solid optical fiber and microstructured optical fibers is the use of pressurization during the fabrication processes. For HCFs, the hollow microstructure of the preform is pressurized during the fiber-drawing process using inert gas applied from the top of the preform. This is necessary both to stop the holes within the microstructure contracting due to surface tension, and to enable precise control of the final fiber geometry [19], [34]. The pressure applied to the microstructure is usually above atmospheric and is controlled via a sealed pressurization system which is connected to the top of the fiber preform, and so, at first-glance it may not be obvious why the final HCF should have an internal structure containing gas at a pressure well below atmospheric. However, as we consider the temperature drop between the furnace and the surrounding environment and the increase in air-filling fraction of the final HCF, a rationale for the sub-atmospheric pressure begins to emerge. To aid this discussion, Fig. 10 shows a schematic of a HCF preform at the neck-down region during the fiber fabrication process where the preform structure is transformed to the fiber geometry by heating at $\sim 2000 \text{ }^\circ\text{C}$ inside a furnace.

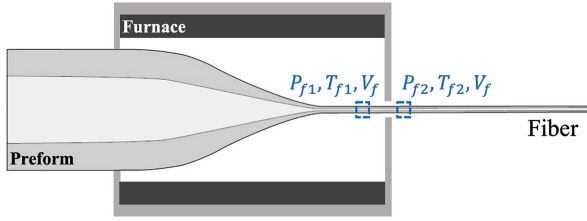


Fig. 10. Schematic of a HCF preform at the neck-down region inside the furnace. The system is vertically positioned and the top of the preform is closed by a pressure interface in reality. P , V and T are the pressure, volume and temperature, respectively. The fiber inside and outside the furnace are represented by f_1 and f_2 , respectively.

A key factor to consider is the impact of the temperature reduction between the inside and outside of the furnace. To estimate the impact of this, we compare the pressure inside two fiber sections; a section of HCF inside the furnace, immediately after the neck-down at a temperature of ~ 1400 °C, which is lower than the softening temperature of silica [35] and a similar fiber section just outside the furnace, at ambient temperature. These fiber sections are highlighted in blue in Fig. 10 and as both sections are after the neck-down region of the preform, and below the softening temperature of silica, we assume these sections to have identical geometry. Mass conservation of the pressurizing gas molecules in the fixed volume, V , of these fiber sections gives:

$$\frac{P_{f1}V_f}{T_{f1}} = \frac{P_{f2}V_f}{T_{f2}} = \text{Constant} \quad (5)$$

where the subscripts f_1 and f_2 represent the fiber inside and outside the furnace, respectively. P and T are the pressure and the temperature, respectively. For the HC-PBGF used in Section III, the hollow core was pressurized with 6 kPa + 1 atm., and if P_{f1} is equal to the pressure inside the preform, the temperature reduction between these fiber sections ($T_{f2}/T_{f1} = 293 \text{ K}/1673 \text{ K}$) decreases the pressure of the final fiber to $P_{f2} = 19 \text{ kPa}$. This estimation is in reasonable agreement with the estimations from the experimental results in this paper, especially considering that all experiments involved some exposure of the fiber to atmospheric pressure pre-measurement.

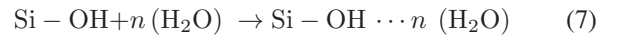
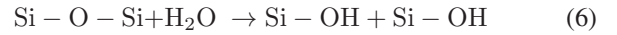
There are also likely to be secondary factors in the sub-atmospheric internal gas pressure related to the gas flow dynamics within the preform and fiber. Typically, the pressurization during the fiber draw yields an air-filling fraction of the final fiber which is significantly increased as compared to that of the initial preform. Considering mass conservation and the very small dimensions of the final fiber (which reduce pressure driven gas flow), the significant change in volume by the expansion of the microstructure could also be a factor in the pressure inside the fiber being a small fraction of the pressure applied to the preform.

The ideal gas law is built upon the following assumptions: (i) molecules have no volume and (ii) there is no attractive force between molecules [36]. It is, therefore, understood that the behavior of a real gas does not obey the ideal gas law when these assumptions are not valid, e.g., under high pressure and low temperature conditions. In the case of the HCF fabrication, the applied pressure is not significantly higher than atmospheric

and the temperature inside the furnace is ~ 2000 °C. Besides, the experimental results showed that the absolute pressure inside the drawn fiber is close to 0 kPa. These facts enable us to use the ideal gas law to estimate the gas pressure inside the preform and the drawn fiber. Although these calculations do simplify the complex gas flow dynamics within the fiber drawing process, they clearly suggest that the temperature, likely in combination with the air-volume changes and the gas flow dynamics during fiber drawing, lowers the internal pressure of the fiber below atmospheric pressure, supporting the experimental results reported here.

B. Interaction of a Silica Surfaces With Gasses in a HCF

Apart from the behavior which can be attributed to the pressure- and diffusion-driven transportation as shown in the gas spectroscopy measurements, the reduction in the recorded absorption of the water vapor during the experiments and after the storage time (with both fiber ends sealed) are highly likely to be due to interaction between water vapor molecules and the inner silica glass surface of the hollow core [37]. The following physical and chemical reactions between water vapor and a silica surface likely occur inside the HCFs [38]:



where n and \cdots represent the number of molecules and the physical bonding, respectively. The reaction of (6) describes the chemical reaction between the water vapor and the silica surface which produces OH groups; these can be either isolated or interacting with each other. Following the formation of a Si-OH surface, excess water vapor physically attaches onto a silica surface as expressed by (7).

Considering runs 1–4 of the absorption measurements, the subsequent experiments indicate that water vapor molecules are gradually adsorbed onto the inner surfaces within the HCF and that the adsorption rate was large when as-drawn HCFs are initially exposed to water vapor in ambient air, but reduced after further exposure. According to the model expressed by (1), the pressure-driven flow stopped at ~ 3 hours after cleaving the sealed ends in the first run. However, a short-term faster increase in the water vapor absorption was also observed at the beginning of the second and third runs, indicating some pressure-driven gas flow into the HCF. This suggests that the internal absolute pressure was reduced during the storage time due to the adsorption of water vapor on the inner silica surface; reduction in absolute pressure has been previously reported as a technique to measure the adsorption rate of water vapor to glass surfaces inside a glass container [39]. The result of a decrease in the internal pressure during the storage is supported by the reduction of the water vapor absorption strength post-storage. On the other hand, this significant reducing trend was not shown by the oxygen and the nitrogen gasses, which provide evidence that these non-polar atmospheric species interact to a significantly lesser extent with the internal fiber surfaces than the water vapor. This suggests that water vapor is a key atmospheric species that needs to be considered when assessing the long-term optical and mechanical performance of a HCF.

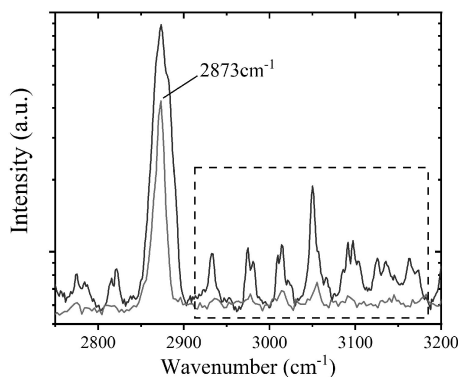


Fig. 11. The Raman Stokes spectra between 2800 cm^{-1} and 3700 cm^{-1} detected from HC-ARFs used in Fig. 6(bottom) and used to repeat the experiment (top). The dashed-square highlights weak features which location agrees with the rotational lines of HCl gas.

C. Initial Gas Compositions in a Post-Fabrication HCF

The low internal pressure shown above indicates that the initial gas concentration inside the hollow core post-fabrication is very small. During a fiber draw, one end of the fiber is connected to the preform, the other end far from the preform (located on the collection drum) is open to atmosphere. With the knowledge from our experiments that as-drawn fibers contain gas at sub-atmospheric pressure, this implies that during the draw, atmospheric gas species will ingress into the fiber from the open end on the drum.

On the other hand, the Raman spectroscopy measurement showed an additional peak which at this point has not been identified as an atmospheric gas species. To understand the origin of this peak, the Raman spectroscopy measurement was repeated using another 36 m of the as-drawn HC-ARF (which was fabricated from the same preform as the HCF used in Fig. 6) with a high resolution of 1.5 cm^{-1} and acquisition time of 1 minute. In Fig. 11 the Raman spectrum which was recorded 21 minutes after opening the ends, from the HC-ARF tested here is compared with the spectra shown in Fig. 6. The high-resolution measurement resolved the shape of the peak at 2873 cm^{-1} , and the peak position and the shape are close to those of the Q-branch vibration of HCl reported in previous studies [26], [27]. In addition, small peaks were clearly observed between 2900 cm^{-1} and 3200 cm^{-1} and the features agree with the S-branch rotational lines of HCl [26], [27]. The presence of HCl gas inside HCFs has been reported previously [16] and therefore the results observed here indicate that the peak at 2873 cm^{-1} was likely attributed to HCl. Yet, more investigation is underway to confirm this.

V. CONCLUSION

The findings in the present work are essential information for the study of the long-term performance of a HCF. The low internal pressure post-fabrication can impact the internal gas composition and internal surface conditions after even short exposure to the atmosphere. Sealing the fiber ends immediately after fabrication is a simple method to maintain the as-drawn conditions as introduced in this work. The subsequent measurements of the gas compositions also highlight the fact that

water vapor molecules from atmospheric gas interact with the internal silica surfaces within the HCF. It has been reported that water vapor can increase the surface OH attenuation of a HCF via chemical reaction with the silica surfaces [40], and excess adsorption of water vapor could have further impact on the fiber's optical and mechanical performance.

The discovery of the low as-drawn pressure could also impact HCF characterization. It has been reported that confinement loss of a HCF can be significantly changed by introducing a small gas-induced differential refractive index between the gas in the hollow core and that in the cladding holes, originating from different gas pressure within these different regions of the microstructure [41]. The nitrogen and oxygen behavior in Fig. 7 shows early potential evidence of this, but further work is underway to evaluate this fully.

All data supporting this study are available from the University of Southampton repository at <https://doi.org/10.5258/SOTON/D1760>.

REFERENCES

- [1] C. Yeh, *Handbook of Fiber Optics: Theory and Applications*, San Diego, CA, USA: Academic, 1990.
- [2] A. Mendez, "Optics in medicine," in *Optics in Our Time*, M. D. Al-Amri, M. El-Gomati, and M. S. Zubairy, Eds., Cham, Switzerland: Springer, 2016, pp. 299–333.
- [3] F. Poletti, M. N. Petrovich, and D. J. Richardson, "Hollow-core photonic bandgap fibers: Technology and applications," *Nanophotonics*, vol. 2, no. 5/6, pp. 315–340, Nov. 2013.
- [4] F. Poletti, "Nested antiresonant nodeless hollow core fiber," *Opt. Exp.*, vol. 22, no. 20, pp. 23807–23828, Oct. 2014.
- [5] H. Sakr *et al.*, "Hollow core NANFs with five nested tubes and record low loss at 850, 1060, 1300 and 1625 nm," in *Proc. Opt. Fiber Commun. Conf. Exhibit.*, San Francisco, CA, USA, 2021, pp. 1–3.
- [6] F. Poletti *et al.*, "Towards high-capacity fibre-optic communications at the speed of light in vacuum," *Nature Photon.*, vol. 7, no. 4, pp. 279–284, Mar. 2013.
- [7] Z. Liu *et al.*, "Nonlinearity-free coherent transmission in hollow core antiresonant fiber," *J. Lightw. Technol.*, vol. 37, no. 3, pp. 909–916, Feb. 2019.
- [8] A. Taranta *et al.*, "Exceptional polarization purity in antiresonant hollow-core optical fibers," *Nature Photon.*, vol. 14, no. 8, pp. 504–510, May 2020.
- [9] P. Jaworski *et al.*, "Picosecond and nanosecond pulse delivery through a hollow-core negative curvature fiber for micro-machining applications," *Opt. Exp.*, vol. 21, no. 19, pp. 22742–22753, Sep. 2013.
- [10] R. Slavík *et al.*, "Ultralow thermal sensitivity of phase and propagation delay in hollow core optical fibers," *Sci. Rep.*, vol. 5, no. 15447, pp. 1–7, Oct. 2015.
- [11] euNetworks Fiber U.K. Limited, "euNetworks deploys Lumenity limited coresmart hollow core fibre cable in London," euNetw. Fiber U.K. Ltd., London, UK, Apr. 14, 2021. [Online]. Available: <https://eunetworks.com/app/uploads/2021/04/euNetworks-deploys-Lumenity-Hollowcore-Fibre-in-London-FINAL.pdf>
- [12] M. Kuwazuru, Y. Namihira, K. Mochizuki, and Y. Iwamoto, "Estimation of long-term transmission loss increase in silica-based optical fibers under hydrogen atmosphere," *J. Lightw. Technol.*, vol. 6, no. 2, pp. 218–225, Feb. 1988.
- [13] K. H. Chang, D. Kalish, and M. L. Pearsall, "New hydrogen aging loss mechanisms in the 1400 nm window," in *Proc. Tech. Dig. Opt. Fiber Commun. Conf., Int. Conf. Integr. Opt. Fiber Commun.*, San Diego, CA, USA, 1999, pp. PD22/1–PD22/3.
- [14] J. L. Mrotek, M. J. Matthewson, and C. R. Kurkjian, "The fatigue of high-strength fused silica optical fibers in low humidity," *J. Non-Crystalline Solids*, vol. 297, no. 1, pp. 91–95, Jan. 2002.
- [15] N. V. Wheeler *et al.*, "Gas absorption between 1.8 and 2.1 μm in low loss (5.2 dB/km) HC-PBGF," in *Proc. Lasers Electro-Opt.*, San Jose, CA, USA, 2012, pp. 1–2.
- [16] J. K. Lyngso, B. J. Mangan, C. Jakobsen, and P. J. Roberts, "7-cell core hollow-core photonic crystal fibers with low loss in the spectral region around 2 μm ," *Opt. Exp.*, vol. 17, no. 26, pp. 23468–23473, Dec. 2009.

- [17] S. Rikimi *et al.*, "Pressure in As-drawn hollow core fibers," in *Proc. OSA Adv. Photon. Congr.*, Washington, DC, USA, Jul. 2020, Paper SoW1H.4 1-2.
- [18] Heraeus, "High purity fused silica tubes for specialty fiber production," Heraeus, Henau, Germany, Apr. 2020. [Online]. Available: https://www.heraeus.com/media/media/hca/doc_hca/products_and_solutions_8/optical_fiber/Fiber_Tubes_EN.pdf
- [19] Y. Chen *et al.*, "Multi-kilometer long, longitudinally uniform hollow core photonic bandgap fibers for broadband low latency data transmission," *J. Lightw. Technol.*, vol. 34, no. 1, pp. 104–113, Jan. 2016.
- [20] J. Henningsen and J. Hald, "Dynamics of gas flow in hollow core photonic bandgap fibers," *Appl. Opt.*, vol. 47, no. 15, pp. 2790–2797, May 2008.
- [21] J. A. Bearden, "A precision determination of the viscosity of air," *Phys. Rev.*, vol. 56, no. 10, pp. 1023–1040, Nov. 1939.
- [22] W. D. Hall and H. R. Pruppacher, "The survival of ice particles falling from cirrus clouds in subsaturated air," *J. Atmosph. Sci.*, vol. 33, no. 10, pp. 1995–2006, Oct. 1976.
- [23] I. Davidson *et al.*, "Tubular anti-resonant hollow core fiber for visible Raman spectroscopy," in *Proc. 6th Int. Workshop Specialty Opt. Fibers Appl.*, Charleston, SC, USA, Nov. 2019, vol. 11206, pp. 1–7.
- [24] T. W. Kelly *et al.*, "Impact of pressure-induced differential refractive index in Raman spectroscopy using hollow-core fibres," in *Proc. Conf. Lasers Electro-Opt. Europe Eur. Quantum Electron. Conf.*, 2021, pp. 1–1.
- [25] H. W. Schrotter and H. W. Klockner, "Raman scattering cross sections in gases and liquids," in *Raman Spectroscopy of Gases and Liquids*, vol. 11, A. Weber, Ed., Berlin, Heidelberg, Germany: Springer, 1979, pp. 123–164.
- [26] G. S. Devendorf, D. Ben-Amotz, and L. E. S. de-Souza, "Raman spectroscopy and theoretical modeling of HCl vibrational frequency shifts in high pressure argon," *J. Chem. Phys.*, vol. 104, no. 10, pp. 3479–3485, Jun. 1996.
- [27] A. Padilla, J. Perez, and A. C. Hernandez, "Vibrational Raman and infrared spectra of polar diatomic molecules in inert solutions. III. Isotropic and anisotropic Raman spectra of HCl in liquid SF₆," *J. Chem. Phys.*, vol. 113, no. 10, pp. 4290–4297, Sep. 2000.
- [28] A. Hamraoui and T. Nylander, "Analytical approach for the Lucas-Washburn equation," *J. Colloid Interface Sci.*, vol. 250, no. 2, pp. 415–421, Jun. 2002.
- [29] N. B. Vargaftik, B. N. Volkov, and L. D. Voljak, "International tables of the surface tension of water," *J. Phys. Chem. Ref. Data*, vol. 12, no. 3, pp. 817–820, Jul. 1983.
- [30] G. S. Kell, "Density, thermal expansivity, and compressibility of liquid water from 0 °C to 150 °C: Correlations and tables for atmospheric pressure and saturation reviewed and expressed on 1968 temperature scale," *J. Chem. Eng. Data*, vol. 20, no. 1, pp. 97–105, Jan. 1975.
- [31] L. Korson, W. Drost-Hansen, and F. J. Millero, "Viscosity of water at various temperatures," *J. Phys. Chem.*, vol. 73, no. 1, pp. 43–39, Jan. 1969.
- [32] S. Takeda, K. Yamamoto, Y. Hayasaka, and K. Matsumoto, "Surface OH group governing wettability of commercial glasses," *J. Non-Crystalline Solids*, vol. 249, no. 1, pp. 41–46, Jul. 1999.
- [33] T. Suzuki, T. Sekine, K. Yamamoto, and K. Fukutani, "Change in the surface OH group on soda lime silicate glass and silica glass after heat treatment in nitrogen atmosphere," *J. Non-Crystalline Solids*, vol. 464, pp. 89–91, May 2017.
- [34] G. T. Jasion *et al.*, "Fabrication of tubular anti-resonant hollow core fibers: Modelling, draw dynamics and process optimization," *Opt. Exp.*, vol. 27, no. 15, pp. 20567–20582, Jul. 2019.
- [35] H. Scholze and N. J. Kreidl, "Technological aspects of viscosity," in *Glass: Science And Technology*, vol. 3, D. R. Uhlmann and N. J. Kreidl, Eds., Orlando, FL, USA: Academic, 1986, pp. 233–273.
- [36] R. Prasad, "Ideal to a real gas, viscosity, conductivity and diffusion," in *Classical and Quantum Thermal Physics*. Cambridge, U.K.: Cambridge Univ. Press, 2016, pp. 49–92.
- [37] S. Rikimi *et al.*, "Long-term behaviour of water vapour absorption in hollow core fibers," in *Proc. 6th Int. Workshop Specialty Opt. Fibers Appl.*, Charleston, SC, USA, 2019, Art. no. 112061U.
- [38] L. T. Zhuravlev, "The surface chemistry of amorphous silica. Zhuravlev model," *Colloids Surfaces A: Physicochemical Eng. Aspects*, vol. 173, no. 1–3, pp. 1–38, Nov. 2000.
- [39] Y. Tuzi, "Sorption of water vapour on glass surface in vacuum apparatus," *J. Phys. Soc. Jpn.*, vol. 17, no. 1, pp. 218–227, Jan. 1962.
- [40] I. Gris-Sanchez and J. C. Knight, "Time-dependent degradation of photonic crystal fiber attenuation around OH absorption wavelengths," *J. Lightw. Technol.*, vol. 30, no. 23, pp. 3597–3602, Dec. 2012.
- [41] T. W. Kelly *et al.*, "Gas-induced differential refractive index enhanced guidance in hollow-core optical fibers," *Optica*, vol. 8, no. 6, pp. 916–920, Jun. 2021.

Shuichiro Rikimi received the B.Sc. degree from the Tokyo University of Science, Tokyo, Japan, in 2016, and the Master of Science degree in optical fibre technologies in 2017 from the University of Southampton, Southampton, U.K., where he is currently working toward the Ph.D. degree with Optoelectronics Research Centre. His research interests include long-term reliability of hollow core fibers, fabrication of hollow core fibers, and gas flow dynamics in hollow core fibers.

Yong Chen (Member, IEEE) received the Ph.D. degree in physics from the University of Bath, Bath, U.K., in 2013. After that, he joined the Optoelectronics Research Centre (ORC), University of Southampton, Southampton, U.K., where he is currently a Senior Research Fellow. His work on the development of novel hollow core fibres played a pivotal role in the foundation of Lumenity Ltd., a spin out company from the ORC, focusing on commercialising hollow core fibres technology. He is currently the Advanced Fibre R&D Manager for Lumenity. He has coauthored more than 100 publications, with a current H-index of 23. His research interests include design, fabrication, and characterization of microstructured optical fibers, postprocessing of conventional and microstructured fibers, mode converters, and nonlinear fiber optics.

Thomas W. Kelly received the M.Phys. degree from the University of Southampton, Southampton, U.K., in 2015, where he is currently working toward the Ph.D. degree with Optoelectronics Research Centre. His research focuses on the using hollow core fibres for Raman gas phase spectroscopy.

Ian A. Davidson received the B.Sc. degree in physics from the University of Edinburgh, Edinburgh, U.K., in 2004, the M.Sc. degree in photonics and optoelectronic devices from the Universities of St. Andrews and Heriot-Watt, Edinburgh, U.K., in 2007, and the Ph.D. degree from Heriot-Watt University, Edinburgh, U.K., in 2013, where he worked on the growth, processing, and characterization of II-VI semiconductor materials. In 2017, he joined the Optoelectronics Research Centre, University of Southampton, Southampton, U.K., as a Research Fellow. He undertaken Postdoctoral research work with Heriot-Watt University, during 2012–2013, and with Stockholm University, Stockholm, Sweden, during 2013–2017. His research focuses on the fabrication and characterisation of micro-structured optical fibres.

Gregory T. Jasion (Member, IEEE) received the M.Eng. degree in aerospace engineering from the University of Southampton, Southampton, U.K., in 2008, and the Ph.D. degree in helicopter dust clouds in 2013. Then, he joined the Microstructured Optical Fibres Group, Optoelectronics Research Centre, as a Specialist in numerical modeling of multiphase flow. He was the recipient of the Research Fellowship from the Royal Academy of Engineering in 2016. He has developed several techniques to model the flow of glass during microstructured fiber draws allowing the team to draw fibers virtually.

Matthew Partridge received the B.Sc. degree in biochemistry from Lancaster University, Lancaster, U.K., and the Ph.D. degree from Cranfield University, Cranfield, U.K., in 2014, on developing fibre optics into molecular sensors. In 2018, he joined Southampton University, Southampton, U.K., and worked on the applications of microstructure fiber in sensing applications. Since 2020, he has been running the science communication website ErrantScience.com and is the Technical Director with Orlef Ltd., a company specialising in point of care diagnostics.

Kerriane Harrington, biography not available at the time of publication.

Thomas D. Bradley (Member, IEEE) received the M.Phys. and Ph.D. degrees from the University of Bath, Bath, U.K., in 2009 and 2014, respectively. His Ph.D. and earlier career research focused on the fabrication, characterization, and loading of gas species in both antiresonant and photonic bandgap hollow-core fibers. In 2014, he joined the Optoelectronics Research Centre, where he is currently a Senior Research Fellow with the micro-structured optical fiber groups. His research interests include the fabrication of low-loss antiresonant hollow-core fibers, development of novel characterization tools for optical fibers, and gas filling in hollow-core fibers. He was the recipient of the Best Early Career Presentation Prize at the EPSRC Manufacturing the Future Conference in 2014.

Austin A. Taranta received the B.Sc. degree in chemical engineering from the Massachusetts Institute of Technology, Cambridge, MA, USA, in 2006. From 2006 to 2016, he was an Optical Engineer with Honeywell Aerospace, Phoenix, AZ, USA, working on the design and manufacture of fiber-optic gyroscopes for high-reliability defense and space applications. In 2016, he joined the Optoelectronics Research Centre, University of Southampton, Southampton, U.K., as a Member of the technical staff. His research interests include the field of optical fibre sensors, especially interferometric and resonant fiber-optic gyroscopes, reliability and harsh environment dynamics of optical fibre performance, and the study of novel properties of hollow-core and other micro-structured fibres for sensing applications.

Francesco Poletti (Member, IEEE) received the Laurea degree in electronics engineering from the University of Parma, Parma, Italy, in 2000, and the Ph.D. degree from the Optoelectronics Research Centre (ORC), Southampton, U.K., in 2007. He is currently a Professor with ORC. He has worked for three years on optical network design with Marconi Communications and for more than ten years on the development of new generations of microstructured optical fibers with ORC. He is the co-founder of Lumenisity Ltd. He has coauthored more than 400 publications in journals and conference proceedings and produced more than ten granted patents. His research interests include the design of photonic bandgap and antiresonant fibers, development of fiber-optic characterization techniques, and fabrication of silica and nonsilica-based fibers and devices. He was the recipient of a Royal Society University Fellowship and European Research Fellowship Consolidator Grant.

Marco N. Petrovich (Senior Member, IEEE) received the Laurea degree in physics from the University of Padua, Padua, Italy, in 1998, and the Ph.D. degree in optoelectronics from the University of Southampton, Southampton, U.K., in 2003. In 1999, he joined the Optoelectronics Research Centre. He has been involved ever since in the development and fabrication of special fibers. Since 2003, he has been working on silica microstructured fibers. He has coauthored more than 250 publications in journals and conference proceedings. His research interests include the development of novel fiber structures, particularly hollow core photonic bandgap and antiresonant fibers, and their application in telecommunications, gas sensing, and power delivery. In 2017, he co-founded Lumenisity Ltd., leading supplier of hollow core fibre cable and connectivity solutions, where he currently leads optical fibre production and R&D engineering. He is a Senior Member of the Optical Society of America, and a Member of the Institution of Engineering and Technology, and an Associate Editor for the IEEE SENSORS JOURNAL. He is a frequent Invited Speaker at international conferences and meetings, including more than 60 invited and post-deadline presentations. He was the recipient of a prestigious Ph.D. studentship awarded by Pirelli Cables Ltd in 1999.

David J. Richardson (Fellow, IEEE) received the B.Sc. and Ph.D. degrees in fundamental physics from Sussex University, Brighton, U.K., in 1985 and 1989, respectively. In 1989, he joined the Optoelectronics Research Centre (ORC), Southampton University, Southampton, U.K. Since 2000, he has been the Deputy Director of the ORC, with responsibility for fiber and laser related activities. His research interests include amongst others optical fiber communications, microstructured optical fibers, and pulsed high-power fiber lasers. He is a prominent figure in the international photonics community, has authored or coauthored more than 1500 research papers, and produced more than 30 patents. Prof. Richardson was an Elected Fellow of the Royal Academy of Engineering in 2009, and a Fellow of the Royal Society in 2018. He is also a Fellow of the Optical Society of America and the Institute of Engineering and Technology. He has co-founded two spin out companies: SPI Lasers Ltd. in 2000 and Lumenisity Ltd. in 2017. He was awarded a Royal Society University Fellowship in 1991 in recognition of his pioneering work on short pulse fiber lasers

Natalie V. Wheeler (Senior Member, IEEE) is currently a Royal Society University Research Fellow with the Optoelectronics Research Centre (ORC), University of Southampton, Southampton, U.K. She has coauthored more than 150 publications, including 33 invited/post-deadline papers and five patents. Her research interests focus on the fabrication and applications of hollow core optical fibres (HCFs). She has led the fabrication of many state-of-the-art HCFs, which have been used in world-leading demonstrations across diverse applications, including telecommunications, high power laser delivery and gas sensing. She holds a prestigious Royal Society University Research Fellowship and now leads ORC activities in gas-filled HCFs, including high sensitivity gas detection and investigations into the long term lifetime and reliability of HCFs. Her work on the fabrication of novel HCFs contributed to the launch of a recent spin out company from the University of Southampton (Lumenisity), which is commercialising HCF technology.